Structural Properties of Atactic Polystyrene of Different Thermal History Obtained from a Multiscale Simulation

Tim Mulder,[‡,†] V. A. Harmandaris,[§] Alexey V. Lyulin,*[,†,‡] N. F. A. van der Vegt,[§] K. Kremer,[§] and M. A. J. Michels[‡,†]

Group Polymer Physics, Eindhoven Polymer Laboratories, Technische Universiteit Eindhoven, P.O. Box 513, 5600 MB Eindhoven, The Netherlands; Dutch Polymer Institute, P.O. Box 902, 5600 AX Eindhoven, The Netherlands; and Max Planck Institute for Polymer Research, Ackermannweg 10, D-55128 Mainz, Germany

Received April 20, 2008; Revised Manuscript Received November 4, 2008

ABSTRACT: A method is presented to obtain well-equilibrated atactic polystyrene (aPS) samples for molecular simulations. The method starts with equilibrating the polymer in the melt at length scales beyond the Kuhn length l_K, using end-bridging Monte Carlo techniques; at this level a (2:1)-coarse-grained description of aPS is being employed. Subsequently atomistic detail is reintroduced, and the sample is equilibrated at the smallest length scales as well. At length scales beyond l_K the simulated polymer chain conformations fulfill the random-coil hypothesis of Flory, and $C_\infty = 8.7 \pm 0.1$ at 463 K. Eventually various glassy samples are created by subjecting the melt sample to different cooling rates. Pair correlations are in agreement with existing X-ray data, and the amount of dihedral angles in the *trans* (*t*) state agrees with NMR data. On the level of dyads, the conformations of racemic dyads agree well with existing NMR results. At the same time, meso dyads conformations do not agree: 65% of meso dyads is in the *gt*/*tg* state (NMR: 80%); 25% is in *tt* state (NMR: <10%). An attempt has been made to relate the observation in simulations, namely that an increase in cooling time causes an increase in yield stress, to effects of the cooling rate on the polymer structure.

1. Introduction

One striking phenomenon originally introduced by Struik[1] in relation to glassy polymers is *physical aging*. It refers to the slow structural relaxation processes, not involving any chemical reactions, in polymer materials below their glass transition. The presence of aging is not restricted to polymers but occurs in any structural glass.

Physical aging is of importance in relation to mechanical properties of materials. The work of Utz et al.[2] showed that for a binary mixture of Lennard-Jones particles the height of the yield peak and the presence or absence of strain softening can be influenced by the heat treatment to which the system is exposed. The presence of physical aging and its influence on mechanical behavior of glassy polymers have been demonstrated by for example Struik et al.[1] and Hasan et al.;[3] slow cooling rates clearly support a high yield stress and the presence of strain softening.

The age of a material increases with time, and the aging is fastest at a temperature just below T_g. The age is determining for the height of the yield peak and the degree of strain softening.[4] The reverse of aging is rejuvenation, which can be accomplished by heating the polymer above T_g and subsequently quenching it into the glassy state again. Alternatively, one can subject the polymer to a mechanical pretreatment, as has been demonstrated by Govaert et al.[5] By mechanical preconditioning, the brittle atactic polystyrene (aPS) is turned into a ductile polymer, albeit that this ductility is temporary. aPS appears to age very fast; already after a couple of minutes the height of the yield peak increases and strain softening returns, and within 2 days the polymer turns brittle. In spite of the observations with respect to the changes in the mechanical behavior, rejuvenation should not be taken too literally; it has been demonstrated by Isner et al.,[6] who use a rugged-energy-landscape model, that states produced by mechanical deformation are generally distinct from states traversed during thermal aging.

The observations mentioned make a polymer like aPS a very interesting material, which indeed has been studied a lot, including simulations at the atomistic level. Lyulin et al. use molecular dynamics simulations to study the stress−strain behavior of aPS, giving, in spite of deformation rates being orders of magnitude larger than in experiments, reasonable values for *E* moduli, yield stresses, and strain-hardening moduli.[7] Aging effects, as seen in stress and energy vs strain plots, have been studied by Lyulin et al.[8] Deformation and segmental relaxation have been explained there in terms of ratios of time scales for cooling. In ref 8 an MD demonstration of the influence of cooling rate on stress−strain behavior is given by stretching uniaxially two samples of 8 chains of 80 monomers each. The samples have been prepared starting from one chain in vacuum, which was allowed to relax under melt conditions. Subsequently, the single chain system was multiplied in all three Cartesian directions, and the resulting system was equilibrated again. The resulting two melt systems of aPS are similar. One of the samples is cooled down through T_g at a rate of 0.01 K/ps and the other at a rate of 0.1 K/ps. Both samples have been subjected to deformation at a rate of 0.025 Å/ps. A more pronounced yield peak and a higher degree of strain softening for the sample cooled down slower have been observed.

Although aging refers to structural relaxation, it is very uncertain what structural properties actually change or evolve during aging. Molecular simulations could be useful to investigate this. Up to date molecular simulations have primarily been used to reproduce experimental data on polymer structures in the melt. Many computational attempts have been made to reproduce the correct conformations of dihedral angles, dyads, triads, etc., in the framework of rotational-isomeric-state (RIS) theories.[9−11] Although conformational distributions are not directly measured, there are NMR data suggesting that model calculations assuming fixed meso dyads with 80% *tg*/*gt* con-

* To whom correspondence should be addressed. E-mail: a.v.lyulin@tue.nl.
‡ Dutch Polymer Institute.
§ Max Planck Institute for Polymer Research.
† Technische Universiteit Eindhoven.

10.1021/ma800873z CCC: $40.75 © 2009 American Chemical Society
Published on Web 12/12/2008

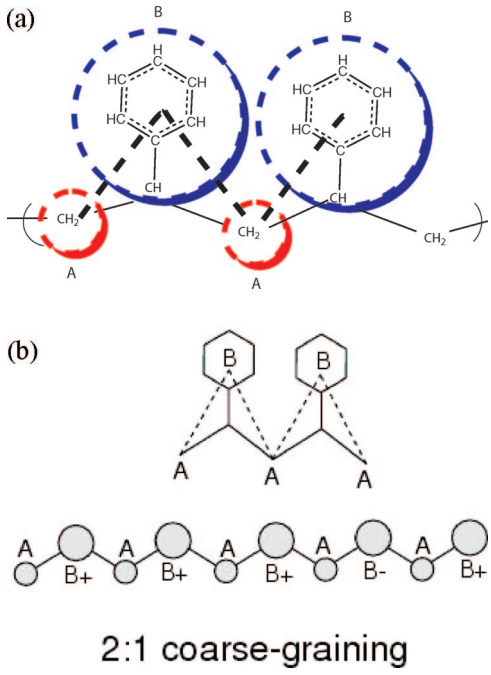

Figure 1. Coarse-grained model of the present study. Two beads represent a monomer. (a) The A bead is located in the center-of-mass of a CH_2 unit, whereas the B bead in the center-of-mass of a $CH(C_6H_5)$ group. The symbols in the beads (b) contain information on tacticity.

formations and less than 10% *tt*, and racemo dyads with more than 50% *tt* and less than 8% $t\bar{g}/\bar{g}t$, are close to experimental reality. In addition, pair-correlation functions have been simulated, for example, by Harmandaris et al.,[12] which reasonably reproduce the X-ray data on aPS from Londono et al.[13] Furthermore, there are attempts to reproduce polymer structures on larger length scales. For example, studies of the intrachain distances between atoms as a function of the number of backbone chemical bonds separating those atoms have been performed by Auhl et al.[15] for a model polymer and by Harmandaris et al.[12,14] and by Spyriouni et al.[16] for aPS. At level of the largest length scales, entanglement networks have been studied by for example Everaers et al.[17] and Tzoumanekas et al.[18] Utz et al.[2] studied the evolution of the pair correlations during the heat treatment of a binary Lennard-Jones system. The number of studies on evolution of structural properties during aging is limited, though.

The main goal of our study is, on the one hand, to reproduce experimental results on the structural properties of aPS in the glassy state at zero stress. On the other hand, we study how the structure evolves during cooling and what the effect of cooling rate is on the structure. Finally, we will see how the properties of the polymer samples under stress depend on aging history. Relevant questions are what properties evolve during aging and what are the relevant length scales. Our approach is the following. First the mapping of the atomistic model onto (2:1)-coarse-grained PS chain is introduced as schematically depicted in Figure 1. Then (2:1) coarse-grained aPS polymer samples are created and equilibrated, as described in detail in our previous publication.[19,20]

Namely, in *p*:1 coarse-grained models, one monomer is represented by p different beads. For $p = 1$, the force field controlling the motions in any degree of freedom in the coarse-grained system is rather simple. One needs bonded potentials controlling bond lengths, bond angles, and dihedrals of the polymer backbone and nonbonded potentials to control interactions of beads in different chains or in the same chain but separated by more than (dependent on details of the model) three or four bonds (excluded-volume effects have to be taken into account properly). For $p = 2$ the monomer consists of two different beads: A beads represent CH_2 groups on the polymer backbone, and B beads represent $CH(C_6H_5)$ groups. Tacticity is incorporated by labeling the B beads with a + or −. The various bond lengths, bond angles, and dihedral angles in the coarse-grained model are controlled by force-field terms that are potentials of mean force of the coarse-grained degrees of freedom. These potentials of mean force have been obtained in atomistic simulations of isolated PS random walks by sampling conformational distribution functions, as also described in ref 19. Clearly, with increasing p necessarily more details are included in the force field; but in addition, incorporation of tacticity can add to its complexity. In the current 2:1 representation of PS tacticity information is also incorporated. In our generalization of the end-bridging MC (EBMC) algorithm for PS, we take this tacticity information into account. The PS samples are thoroughly equilibrated on this coarse-grained level first using the EBMC method. The starting point was an EBMC algorithm designed for and particularly efficient in equilibrating systems of polyethylene chains of realistic molecular weight ($M_w \gg 1$ kDa) in the melt (see ref 21). All moves described there (as local moves such as flips, end rotations and concerted rotations inside the chain, and nonlocal moves such as reptations and end bridging) could be and are used again. Subsequently, atomistic details are reintroduced, after which the structures are equilibrated at the smallest length scales, i.e., down to the chemical bond length, using united-atom molecular dynamics simulations. Afterward, the equilibrated aPS melt samples are cooled below T_g at the two different cooling rates (0.01 and 0.1 K/ps) in MD. Finally, the glassy aPS samples are used for MD production runs, from which structural properties have been calculated. Dihedral distributions and dyad conformations have been calculated as well as distance factors as measured by e.g. Robyr and Suter.[22] In addition, the distribution of angles between phenyl rings have been determined as a function of the spatial distance between them. Also, pair-correlation functions have been calculated and compared to the data of Londono et al.[13] And finally, intrachain distances have been computed to examine the longer length scales.

In section 2 the details of the reinsertion of atomistic detail are described as well as further details of the sample-building process and the production runs. In section 3 the aPS structures, in the melt and in the glass, are compared with various results from the literature, and details regarding the calculation of various distributions and quantities are provided. In section 4 the samples resulting after the different cooling rates are compared in their structural details. Finally, conclusions are presented in section 5.

2. Reinsertion of Atomistic Detail

An aPS sample consisting of (2:1)-coarse-grained polymer chains has been prepared following the method described in ref 19, starting from initial chain configurations, and further equilibration using the end-bridging Monte Carlo algorithm initially developed to simulate polyethylene melts, and modified here for aPS. The polymer sample prepared consists of 50 chains within a uniform mass distribution between $\bar{X}(1 - \Delta)$ and $\bar{X}(1 + \Delta)$ with an average chain length of $\bar{X} = 100$ monomers, and the value of the standard deviation normalized with the mean is $\Delta = 0.5$. The pressure is 1 bar, and the temperature is 463 K, which is well above the glass-transition temperature (experimentally observed values for T_g are around 373 K). Usually the value of T_g is defined by simulating (at atmospheric pressure) the temperature dependence of the specific volume. The dependence of T_g on the cooling rate has been determined experimentally[23] for some metallic glasses and polymers (poly-

(methyl methacrylate), polycarbonate resin). Assuming that the relaxation time of the system follows a Vogel−Fulcher dependence on temperature, it was found that the glass-transition temperature logarithmically increases with cooling rate. It was generally concluded that the values of T_g determined from MD simulations are displaced, as expected, to somewhat higher temperatures than the longer time experimental values, but the displacements are minor. Lyulin et al.[24] show a logarithmic dependence of T_g on cooling rate, and for PS they find for typical cooling rates in simulations (0.1−0.01 K/ps) values for T_g in the range 390−400 K.

In order to be able to calculate the structural properties mentioned in the Introduction and to check the effect of the cooling rate on these properties, reintroduction of the atomistic detail into the (2:1)-coarse-grained description is needed. The resulting structures have been used in united-atom MD production runs afterward. The back-mapping consists of three steps involving a geometric construction, an energy minimization, and a very short (50 ps) MD run. The calculated pair distribution functions (see below) were in an excellent agreement with the experiment, thus justifying the length of this additional MD run. The whole procedure is described in detail in the next few paragraphs of this section.

In the first step C atoms are reintroduced. In the (2:1)-coarse-grained description of aPS, the CG atoms of type A represent a CH_2 unit and the CG atoms of type B represent a CHC_6H_5 unit. In order to reconstruct the seven C atoms represented by every B atom, one needs to use the positions of the coarse-grained beads and the previously inserted atoms as well as of the average distances between the different types of atoms $d_{ij,av}$ within the same monomer or monomers nearby (i and j represent any type of C atom or CG atom). These distances have been obtained from atomistic simulations.[12] C atoms are now introduced in trial positions, from which the distances d_{ij} to three atoms nearby are calculated. Subsequently, the length differences $d_{ij} - d_{ij,av}$ are minimized using a quasi-Newton algorithm.[25] Note here that the above back-mapping scheme, as any other scheme that introduce more detail, is not unique; i.e., starting slightly different might lead to slightly different states. This is expected since one CG configuration corresponds to a set of atomistic states. The back-mapping procedure creates one out of them.

In the second step the united-atom polymer sample is equilibrated for 50 ps in MD, still at 463 K and 1 bar, using a soft-core potential for the repulsive van der Waals interactions to prevent large local conformational distortions due to spatial overlap of atoms:

$$U_{LJ,soft}(r) = \begin{cases} 24\epsilon(1 - r/\sigma) + 228\epsilon(1 - r/\sigma)^2 & r \le \sigma \\ 4\epsilon((\sigma/r)^{12} - (\sigma/r)^6) & r > \sigma \end{cases} \quad (1)$$

The complete force field with all details has been taken from Mondello et al.[26] and also explained in detail elsewhere.[27] The pressure is controlled using the Berendsen barostat[28] ($\beta_p = 0.2$, where β_p is the ratio of the isothermal compressibility and the time constant of the barostat), and the temperature is controlled via the collisional-dynamics thermostat[29] ($\lambda = 3$ ps, $m_0 = 1$ Da).

After equilibration with the soft-core potential, in the third step of the back-mapping procedure, the full Lennard-Jones potential is introduced, and a 50 ps MD simulation is performed. From the obtained trajectories structural properties are calculated and compared to data from literature; the results are given in section 3. Finally, the sample is used for two different cooling simulations, one at a rate of 0.01 K/ps and the other at 0.1 K/ps, which are typical state-of-art cooling rates employed in atomistic molecular simulations.[24] The two resulting aPS glass samples are compared with regard to their structural properties, calculated from 50 ps simulation runs at the final temperatures; this is discussed in section 4.

3. Structural Properties of aPS Resulting from the Multiscale Preparation Method

The main purpose of the coarse-graining and the connectivity-altering Monte Carlo method described in ref 19 was to improve the equilibration at longer length scales, beyond the level of the Kuhn length. To verify to what extent this was successful, the intrachain distances, i.e., the average distance between monomers on the same chain separated by N backbone chemical bonds, have to be verified. For this purpose the characteristic ratio C_N has been studied as a function of the number of backbone atoms:

$$C_N = \left\langle \frac{R^2(N)}{Nl^2} \right\rangle \quad (2)$$

where $R^2(N)$ is the squared distance between atoms separated by N backbone chemical bonds and l the length of the chemical bond in the aPS backbone.

In Figure 2a C_N of aPS has been given, as obtained from the simulations, at three different temperatures: one above T_g (=373 K[30]) and two below T_g. For all temperatures R/Nl^2 tends to a constant value for large N, in agreement with Flory's random-coil hypothesis.[31] In Figure 2b−d the values of C_∞ have been determined from linear fits to the curves of C_N vs $1/N$. (Flory[31] shows for freely rotating chains that $\langle R^2(N)/Nl^2 = C_\infty(1 - \alpha/N)\rangle$, with α independent of N. Because the aPS polymer chains studied here could be mapped onto freely rotating chains, linear fits of C_N vs $1/N$ data are used here as well.) At $T = 463$ K we obtain $C_\infty = 8.7 \pm 0.1$, which compares well to the value 8.5 predicted from literature at that temperature (for aPS $C_\infty = 9.85$ at 300 K and $d(\ln C_\infty)/d(\ln T) = -0.9 \times 10^{-3}$).[30]

At lower temperature the value of $C_\infty = 9.85$ is not approached. Whereas C_∞ should increase during cooling, this is not observed in our simulations; it even decreases a few percent. For $T = 300$ K (after cooling from 463 K at a rate of 0.1 K/ps) a value of 8.3 ± 0.1 has been found and for $T = 323$ K (after cooling from 463 K at a rate of 0.01 K/ps), 8.5 ± 0.1. These observations can be understood by realizing that the polymer chains have no chance to undergo conformational changes at length scales beyond the Kuhn length during cooling by either cooling rate employed here; probably the simulated changes in intrachain distances at those length scales can be largely attributed to the increase in density during cooling (the size of the sample reduces by 1.5% for both cooling rates).

To make a comparison at length scales of a few monomer segments or smaller, the pair-correlation function g_{rem} has been studied. This correlation function, which excludes correlations between atoms separated by fewer than three chemical bonds or atoms belonging to the same phenyl ring, has been extracted by Londono et al.[13] from X-ray measurements on various polymers, among which aPS. In the left part of Figure 3 g_{rem} has been given for the simulation in the glassy state ($T = 323$ K), together with the data of Londono et al. The agreement of the simulations with the experimental data is excellent.

In addition to pair correlations, distributions of dihedral angles have been determined from the simulations (see Figure 5); dihedral angles are defined as explained in Figure 4. According to the NMR measurements of Dunbar et al.,[32] at room temperature, the amount of dihedral angles in the t state is 68 ± 10%. The results from our simulations are in agreement with this result of Dunbar et al.; the agreement is best for the simulated aPS structure that has been created with the slowest cooling rate (0.01 K/ps).

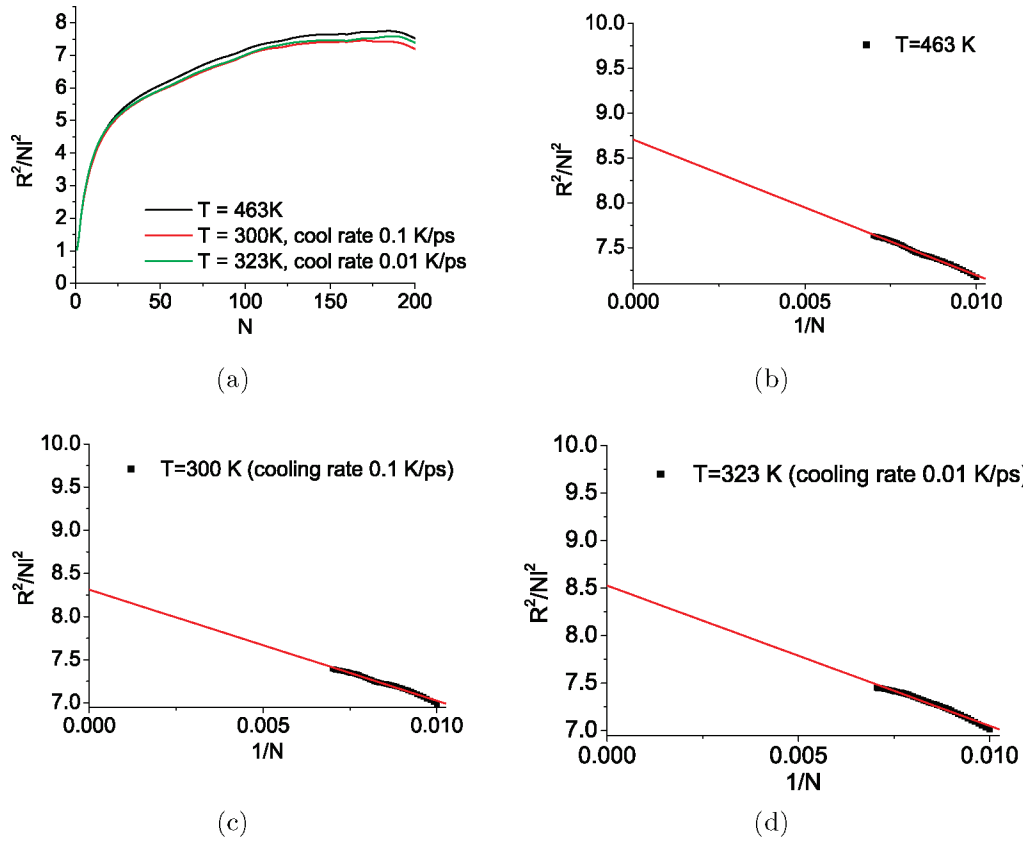

Figure 2. Internal distance distributions (a) in the melt at $T = 463$ K and in the glass at $T = 300$ K and $T = 323$ K. All curves tend asymptotically to a constant value, in accordance with Flory's random-coil hypothesis. The values of C_∞ have been determined for all three temperatures from linear fits to the internal distance distributions; see (b)−(d).

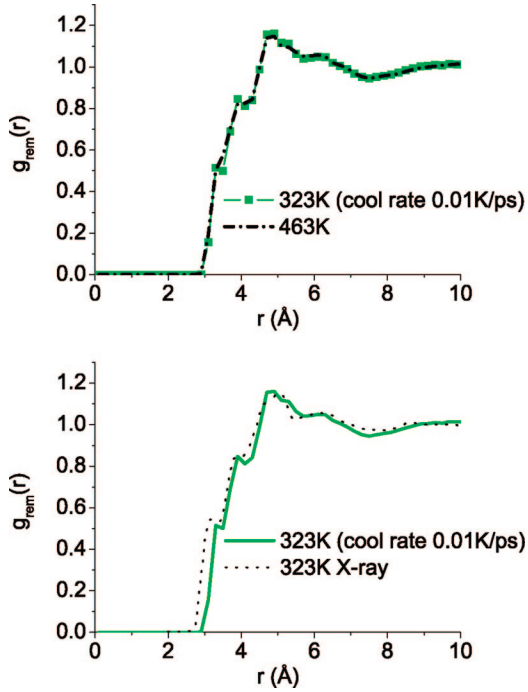

Figure 3. Pair-correlation functions g_{rem} in the melt at $T = 463$ K and in the glass at $T = 323$ K (above) and comparison with the results of Londono et al.[13] (below). In these functions the trivial contributions from atoms separated by fewer than three chemical bonds or between atoms in the same phenyl ring have been left out.

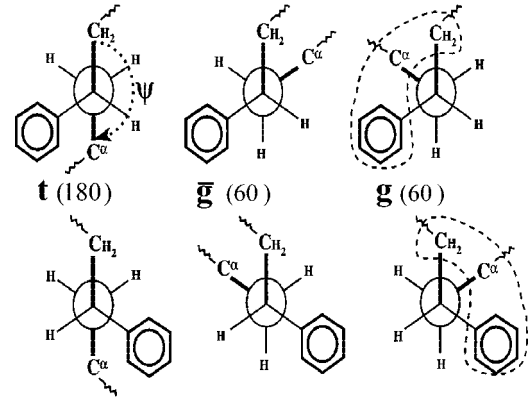

Figure 4. All backbone dihedrals (determined by positions of four consecutive atoms in the backbone), viewed in the same direction, that is, always starting from a CH_2 unit: $CH_2-CH(C_6H_5)-CH_2-CH(C_6H_5)$. The direction of positive orientation is such that sterically equivalent conformations are assigned the same dihedral angle.

Apart from having a correct dihedral angles distribution, a simulated polymer structure must also be able to capture the correct distribution of dyad conformations, determined by two consecutive dihedral angles in the polymer chain's backbone. In Table 1 the percentages of dyads in the various possible conformations are given for all simulated aPS structures. A good way of testing whether these dyad-conformational distributions are close to those in experimental reality is by calculating so-called geometrical rate factors, which can be measured by solid-state NMR. These geometrical rate factors $g(\omega_A,\omega_B)$, which are very sensitive to the distribution of dyads over their various possible conformations, determine the rate of magnetization exchange between two spin packets A and B that have their chemical shift anisotropy (CSA) tensor differently oriented in the static magnetic field $\vec{B}_0$ and therefore resonate at different frequencies, ω_A and ω_B.[22] In various experimental studies to

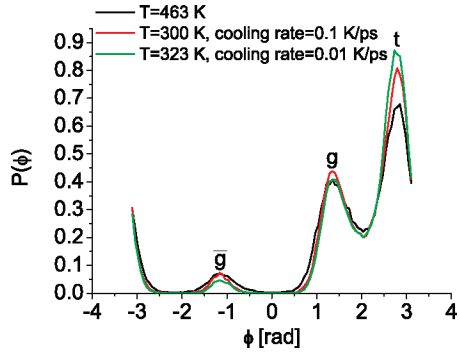

	T=463K	T=300K (0.1K/ps)	T=323K (0.01K/ps)
t	56.2	60.2	63.9
$\bar{g}$	5.4	3.7	2.5
g	38.4	36.1	33.6

Figure 5. Distribution $P(\phi)$ of dihedral angles in the melt at 463 K and in the glassy state at 323 and 300 K. The percentages of t, g, and $\bar{g}$, resulting from integrating $P(\phi)$ over $(-\pi, -\pi/3]$, $(-\pi/3, \pi/3]$, and $(\pi/3, \pi]$, respectively, are given in the table.

Table 1. Conformations of Dyads at 463 K in the Melt and in the Glassy State at 300 and 323 K

		T = 463 K, %	T = 300 K (0.1 K/ps), %	T = 323 K (0.01 K/ps), %
meso	tt	19.8	24.8	27.7
	$\bar{g}\bar{g}$	0.0	0.0	0.0
	gg	5.5	4.3	4.1
	$\bar{g}$t/t$\bar{g}$	7.5	5.8	4.2
	gt/tg	64.9	63.5	63.2
	$\bar{g}$g/g$\bar{g}$	2.3	1.6	0.8
racemic	tt	43.8	48.9	55.2
	$\bar{g}\bar{g}$	0.0	0.0	0.0
	gg	24.6	22.3	18.3
	$\bar{g}$t/t$\bar{g}$	6.1	3.0	1.9
	gt/tg	19.4	21.4	21.6
	$\bar{g}$g/g$\bar{g}$	6.1	4.4	3.0

determine geometrical rate factors for aPS,[22,33,34] aPS with ^{13}C labels at position 1 in the phenyl group has been used (see Figure 6). The orientation of the phenyl ring with respect to the external magnetic field $\vec{B}_0$ determines its resonance frequency ω. $g(\omega_A,\omega_B)$ determines the rate at which spin exchange takes place between an ensemble of phenyl groups with a particular orientation with respect to the external magnetic field that corresponds to a Larmor frequency ω_A and an ensemble of phenyl groups with an orientation with respect to $\vec{B}_0$ that corresponds to a Larmor frequency ω_B. For an ensemble of N interacting spins the geometrical rate factor g_{AB} is given by

$$g(\omega_A, \omega_B) = \frac{N}{n_A n_B}\left(\frac{\mu_0}{4\pi}\frac{\hbar\gamma^2}{2}\right)\sum_i^{n_A}\sum_j^{n_B}\left(\frac{1 - 3\cos^2\theta_{ij}}{r_{ij}^3}\right)^2 \quad (3)$$

where n_A and n_B are the numbers of spins with frequencies in small intervals around ω_A and ω_B, respectively. The vacuum magnetic permeability is μ_0, the gyromagnetic ratio is γ, r_{ij} is the distance between spins i and j, and θ_{ij} is the angle between the internuclear vector and the static magnetic field $\vec{B}_0$. The geometrical rate factor provides information on local orientational order between the phenyl rings. In absence of such order a 2D plot of $g(\omega_A,\omega_B)$ will be totally flat; deviations from flatness indicate preferred angles between spatially proximate phenyl groups. A quantity that is similar to the geometrical rate factor but that is measured under magic-angle spinning (MAS) conditions[35] (where the angular dependence drops out) is the distance factor. The distance factor f_d is defined as

$$f_d(\omega_1, \omega_2) = 4\pi\rho\int_0^\infty g_{12}(r)r^{-4}\,dr \quad (4)$$

where ρ is the density of the labeled spins and $4\pi g_{12}(r)r^2/V$ is the probability density to find a spin with resonance frequency between ω_1 and $\omega_1 + d\omega_1$ and a spin with resonance frequency between ω_2 and $\omega_2 + d\omega_2$ at a distance between r and $r + dr$; V is the volume of the sample. The sensitivity of the distance factor to local packing comes from the dependence of the resonance frequencies on the orientation of the molecular fragments with respect to the static magnetic field. The distance factor spectra from disordered amorphous samples would be flat, $f_d(\omega_1, \omega_2)$ = constant; polycrystalline solids, which are locally perfectly ordered, give rise to sharp peaks.

The rate constants $R(\omega_A,\omega_B)$ ($\sim g(\omega_A,\omega_B)$) for polarization transfer between phenyl rings, as obtained from the simulations at the various temperatures, are shown in Figures 7a−c; those reported by Robyr et al.[22] are shown in Figure 7d. Clearly there exists local order between the phenyl rings, and the order is exaggerated in the simulations, as can be seen from the stronger deviations from a flat profile for the simulations than for the experiments. To extract more information from these rate factors, one should look into separate contributions from different types of dyads and contributions from orientational correlations between phenyl groups in different chains. Some experimental results on the separate contributions of meso and racemic dyads already exist.[33]

Robyr, Gan, and Suter[33] showed that distance factors, calculated using RIS models with for meso dyads more than 80% *tg*/*gt* and less than 10% *tt* and for racemic dyads more than 50% *tt* and less than 8% *t*$\bar{g}$/$\bar{g}$*t*, approach experimental distance factors very reasonably. From our simulations we obtain conformations of racemic dyads that agree with these results. For the meso dyads the percentage of dyads in *tg*/*gt* found in the simulations, 63%, is too low; the amount of meso dyads in *tt*, 28%, is much too high.

The reason for the discrepancies between the simulation results for meso-dyad conformations and the results of Robyr et al. is not obvious. However, some insight into the causes of the discrepancies may be obtained from comparing the aPS structures prepared by the methods described in this paper to a similar approach that was followed by Spyriouni et al.[16] In our work aPS sample preparation is initiated with equilibration at the (2:1) level of coarse graining, followed by reinsertion of

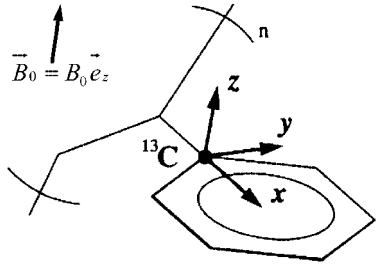

Figure 6. A C^{13}-labeled phenyl ring in an external magnetic field $\vec{B}_0$. The carbon atoms at positions 1 in the phenyl ring are ^{13}C and are thus sensitive to NMR. The orientation of $\vec{B}_0$ with respect to the phenyl ring determines the resonance frequency of the ^{13}C atom.

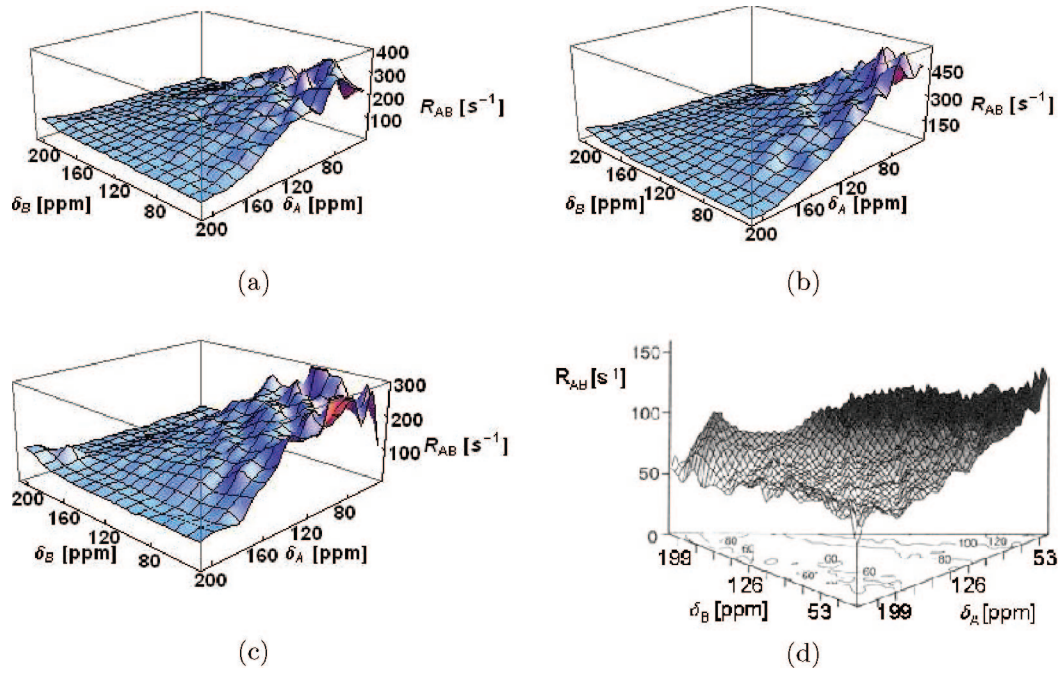

Figure 7. Rate constants for polarization transfer obtained from the simulations (a−c) at 463 K (a), 323 K (b), and 300 K (c) and from experiments at 295 K by Robyr[22] (d). The distance factors at 300 K (c) compare reasonably to the distance factors measured by Robyr et al. (d). Further improvement of the dyad statistics (see discussion on dyad conformations) is needed to obtain better agreement between distance factors as obtained from experiment and simulation. In (a) through (c) the parts-per-million scale ($\Delta f/f \times 10^6$) has been used; in (d) the kHz (Δf) scale, where Δf is the shift of the NMR resonance frequency with respect to the resonance frequency f of the standard reference TMS (tetramethylsilane). For details on both scales see for example ref 22 or 36).

atomistic detail and equilibrating locally afterward. Spyriouni et al. start by equilibrating using a 1:1-coarse-grained model of aPS. Subsequently, a backmapping scheme, i.e., a scheme for reinsertion of atomistic detail, has been used that is necessarily much more complicated than ours, as their coarse-grained model is further away from the atomistic one than ours. Spyriouni et al. report on the conformational properties of their PS samples at a temperature of 500 K an overall amount of dihedrals in the *t* state of around 60%, which is comparable to our 56% at 463 K. And considering the temperature difference, the conformational data found by Spyriouni et al. at 500 K are probably also in agreement with the experimental result of Dunbar et al.[32] at room temperature (68 ± 10% of the dihedrals in the *t* state). For the conformations of dyads Spyriouni et al. observe the following. The amount of meso dyads in the *gt*/*tg* conformation is 60% and of all racemic dyads 45% is in the *tt* conformation. These results are again comparable to our results (see Table 1). The agreement between the present results on conformational properties of PS and those of Spyriouni et al. is remarkable. The fact that in both Spyriouni and our simulations the same force field for the atomistic simulations has been used does not trivially explain the agreement between both data.

4. Structural Properties Obtained from the Different Cooling Rates

After checking the simulated properties vs experimental knowledge, we would like to compare the different properties of the sample created by slow cooling from the melt (at 0.01 K/ps to a final temperature of 323 K) and the sample created by fast cooling (0.1 K/ps to a final temperature of 300 K). As already observed in the Introduction, the cooling rate is reflected in the mechanical behavior. The stress−strain curves obtained using two different cooling rates are different, primarily in the height of the yield peak, the sample resulting from the lower cooling rate giving the highest yield stress as shown in ref 8. From the previous discussion of the intrachain distances distribution, it became already clear that chain conformations change little at the long length scales, and intrachain distances essentially scale with size of the sample.

At the level of pair-correlation functions, one observes a bit sharper peaks at lower temperatures (see Figure 3, lower panel). Especially peaks at the length scales below 4−5 Å become sharper, which is a signature of increased local order upon cooling. The influence of cooling rates, however, on the pair-correlation functions is hardly noticeable (see Figure 3, left panel). This information is very general and does not give much insight. It would be more interesting to look at specific, carefully chosen correlations, such as correlations between atoms in spatially close phenyl rings, either in the same chain or in different chains.

As an example we studied the distribution of angles β between phenyl planes as a function of their distance. The distribution $P(\beta)/\sin\beta$ is given in Figure 8. Small angles are preferred, both at high temperature (463 K) and in the glassy state. For temperatures below the glass transition this ordering effect is more pronounced. Again, the influence of cooling rate is very small; compare parts b and c of Figure 8. Probably for length scales smaller than 5 Å, the only effect is that the thermal fluctuations of angles β around their average values become less as the temperature is decreased. For length scales above 5 Å no changes are observed; both above and below the glass transition, no preferred angles are present. This could mean that in real aPS at distances beyond 5 Å no orientational correlation between phenyl rings exists. However, alternatively it could mean that although there exist such correlations in real aPS, this is not seen in the simulations because of the huge cooling rates.

The dihedral angle distributions (see Figure 5) show an increase, upon cooling, in the number of dihedral angles in the *t* state, at the cost of both dihedral angles in the *g* state and in the $\bar{g}$ state. These effects are almost twice stronger for the slower cooled sample than for the faster cooled one. These effects are

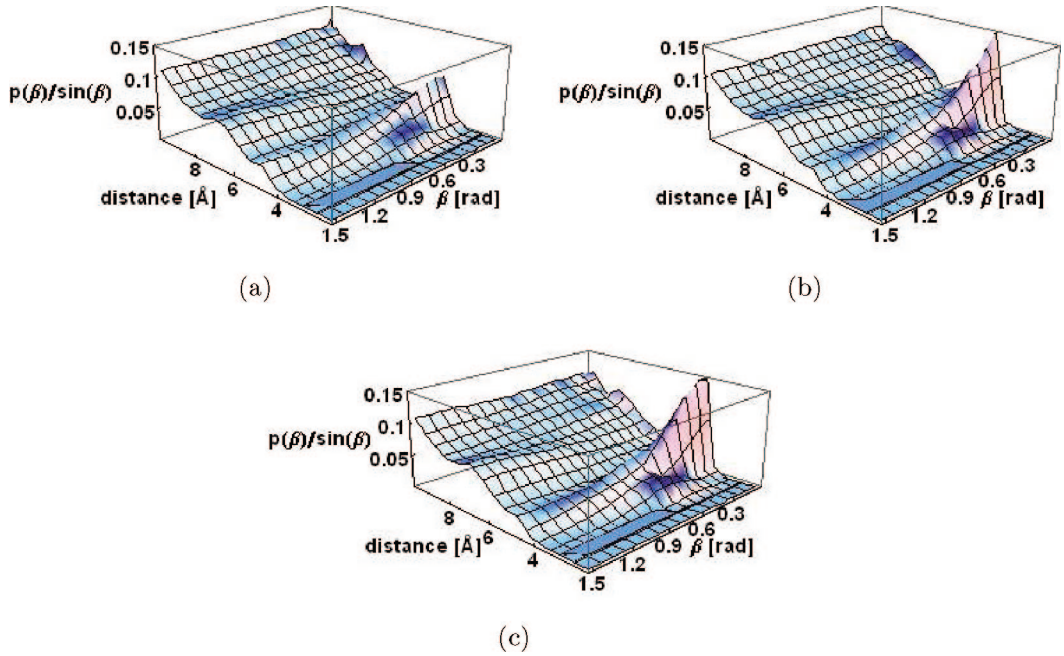

Figure 8. Distribution $P(\beta)/\sin\beta$ of angles between phenyl groups as a function of their distance, for the aPS sample above T_g at 463 K (a) and for the aPS samples below T_g resulting from the cooling with 0.1 K/ps (b) to 300 K and from the cooling with 0.01 K/ps to 323 K (c). For distances shorter than 5 Å small angles between phenyl planes are preferred; this effect is especially pronounced below T_g. The cooling rate seems hardly of influence on this type of ordering.

also seen in dyad conformations (see Table 1). For the racemic dyads, upon cooling, an increase of 11% in the number of dyads in the *tt* conformation is seen and a decrease in essentially all other conformations. With regard to the meso dyads, the amount of *tt* dyads increases by 8%. Again the cooling rates are important.

Although interesting, the observations with respect to cooling rate differences still do not answer the question what structural properties are important to aging and how differences in the yield peak (see ref 8) have to be understood. As a next step, one should subject the samples resulting from both cooling rates to deformation and monitor the evolution of structural properties (primarily of dihedral distributions and distributions of dyad conformations); a major question is whether these structural properties of both samples become equal after strain softening, beyond which the stress−strain curves seem to coincide.

5. Conclusions

A new method to generate aPS polymer samples has been studied. In a first stage the aPS is modeled using a (2:1)-coarse-grained description; i.e., PS monomers are described by two coarse-grained atoms. At this level of description the polymer has been equilibrated using recently developed end-bridging Monte Carlo techniques. After this equilibration at a coarse-grained level, atomistic detail (only hydrogen atoms are left out) has been reintroduced. Subsequently equilibration above T_g has been carried out. Finally, to obtain room temperature aPS, the sample is cooled through the glass transition at 373 K. Two different cooling rates have been used to study their effect on structural evolution.

On the longest length scales, beyond the Kuhn length, the sample preparation resulted in polymer conformations in agreement with Flory's random-coil hypothesis, as could be concluded from the fact that the characteristic ratio C_N goes asymptotically to a constant value as N becomes large. Moreover, the value $C_\infty = 8.7 \pm 0.1$ found for the sample above T_g is similar to the literature value.[30] At temperatures below T_g the conformations at the longest length scales are essentially the same; for the samples below T_g the values obtained for C_∞ are 8.5 ± 0.1 and 8.3 ± 0.1. The slight decrease in C_∞ can be attributed to the decrease of the sample volume upon cooling.

The pair correlations found are in excellent agreement with X-ray data.[13] On top of that, dihedral angle conformations as predicted by NMR[32] are reproduced in the simulations reported here. At the level of dyad conformations, important differences are observable between the simulated aPS structures and existing NMR results.[22] The conformations of racemic dyads found in the simulations are in agreement with the experimental data. For the meso dyads large differences can be observed; whereas NMR data suggest more than 80% in the *tg*/*gt* and less than 10% in the *tt* conformations, the simulated structures show only 65% of the meso dyads in *tg*/*gt* and as much as 25% in *tt*. The cause of these differences is not clear.

Another simulational approach to prepare aPS, by Spyriouni et al.,[16] comparable to the one presented here, starts with equilibration of aPS at a 1:1-coarse-grained level, also using connectivity-altering Monte Carlo. After equilibrating the coarse-grained polymer, a complicated backmapping scheme is used to reinsert atomistic details. Finally, the aPS sample is equilibrated at $T = 500$ K. In spite of the conceptual similarity, there are obvious differences with our approach. In the present approach we employ a more detailed description of the aPS monomer unit, and as a consequence our backmapping is simpler. In spite of these clear technical differences, both approaches perform equally well with regard to reproducing experimental observations on structural properties of aPS. Both the method of Spyriouni and the method presented here are successful in reproducing polymer conformations at length scales beyond the Kuhn length. The distributions of dihedral angles are in agreement with experiments as well.[32] Experimental data on dyad conformations are not correctly reproduced in both approaches.

Finally, the structures resulting from the preparation method presented here have been used to look into effects related to aging. An attempt has been made to relate differences in stress−strain behavior observed between two samples prepared by using different cooling rates to differences in the structures of both samples. At the level of the pair-correlation function,

sharper peaks indicating stronger local ordering have been observed for temperatures below T_g than for temperatures above T_g. However, no influence of the cooling rate was seen. Also, the distribution of angles between phenyl rings as a function of the distance between the rings did not reveal any influence of the cooling rate. The only clear differences were observed in the distributions of dihedrals angles and consequently in the distributions of the meso and racemic dyads over their various possible conformations.

The main goal of this paper is to present the whole multiscale methodology and to check how structural properties change with cooling rate. Not all differences in the structural properties between the two samples, obtained using two different cooling rates, are very pronounced; however they are significant. We do observe the differences between the samples obtained using two different cooling rates, namely, (i) the stress−strain curves obtained using two different cooling rates are different, primarily in the height of the yield peak; (ii) the characteristic ratio for a polymer prepared with lower cooling rate is slightly larger; (iii) the distribution of dihedral angles as well as of the dyads conformations changes with cooling rate: the number of dihedrals in the trans state is increasing upon cooling. This effect is almost twice stronger for the slower cooled sample than for the faster cooled one.

We also have shown that with decreasing the temperature the characteristic ratio is also decreasing in contrast with experimental data. The reason is the very high cooling rates compared to the experimental ones. Because of that, the chains do not have time to equilibrate at the level of the end-to-end distance. This can be seen by the values reported for the different cooling rates: samples after cooling with a rate 0.1 K/ps shown $C_\infty = 8.3$ whereas samples after cooling with a rate 0.01 K/ps (thus giving more time for the chains to equilibrate) shown $C_\infty = 8.5$.

Our results do show small structural differences for the samples obtained using two different cooling rates. In a possible follow-up study of aging one should focus on the evolution (during deformation) of structural properties, especially dihedral angle distributions and distributions of dyad conformations, in samples obtained from different cooling rates; a key question is whether beyond strain softening, where stress−strain curves coincide, differences in structural properties have been erased.

Acknowledgment. This work forms part of the research programme of the Dutch Polymer Institute (DPI), project 487.

References and Notes

(1) Struik, L. C. E. *Physical Aging in Amorphous Polymers and Other Materials*; Elsevier: Amsterdam, 1978.
(2) Utz, M.; Debenedetti, P. G.; Stillinger, F. H. *Phys. Rev. Lett.* **2000**, *84*, 1471.
(3) Hasan, O. A.; Boyce, M. C. *Polymer* **1993**, *34*, 5085.
(4) van Melick, H. G. H.; Govaert, L. E.; Raas, B.; Nauta, W. J.; Meijer, H. E. H. *Polymer* **2003**, *44*, 1171.
(5) Govaert, L. E.; van Melick, H. G. H.; Meijer, H. E. H. *Polymer* **2001**, *42*, 1271.
(6) Isner, B. A.; Lacks, D. J. *Phys. Rev. Lett.* **2006**, *96*, 025506.
(7) Lyulin, A. V.; Vorselaars, B.; Mazo, M. A.; Balabaev, N. K.; Michels, M. A. J. *Europhys. Lett.* **2005**, *71*, 618.
(8) Lyulin, A. V.; Michels, M. A. J. *Phys. Rev. Lett.* **2007**, *99*, 085504.
(9) Yoon, D. Y.; Sundararajan, P. R.; Flory, P. J. *Macromolecules* **1975**, *8*, 776.
(10) Rapold, R. F.; Suter, U. W. *Macromol. Theory Simul.* **1994**, *3*, 1.
(11) Rehahn, M.; Mattice, W. L.; Suter, U. W. *Adv. Polym. Sci.* **1997**, 131–132.
(12) Harmandaris, V. A.; Adhikari, N. P.; Van der Vegt, N. F. A.; Kremer, K. *Macromolecules* **2006**, *39*, 6708.
(13) Londono, J. D.; Habenschuss, A.; Curro, J. G.; Rajasekaran, J. J. *J. Polym. Sci., Part B* **1996**, *34*, 3055.
(14) Harmandaris, V. A.; Reith, D.; VanderVegt, N. F. A.; Kremer, K. *Macromol. Chem. Phys.* **2007**, *208*, 2109.
(15) Auhl, R.; Everaers, R.; Grest, G. S.; Kremer, K.; Plimpton, S. J. *J. Chem. Phys.* **2003**, *119*, 12718.
(16) Spyriouni, T.; Tzoumanekas, C.; Theodorou, D. N.; Müller-Plathe, F.; Milano, G. *Macromolecules* **2007**, *40*, 3876.
(17) Everaers, R.; Sukumaran, S. K.; Grest, G. S.; Svaneborg, C.; Sivasubramanian, A.; Kremer, K. *Science* **2004**, *303*, 823.
(18) Tzoumanekas, C.; Theodorou, D. N. *Macromolecules* **2006**, *39*, 4592.
(19) Mulder, T.; Harmandaris, V. A.; Lyulin, A. V.; Van der Vegt, N. F. A.; Vorselaars, B.; Michels, M. A. J. *Macromol. Theory Simul.* **2008**, *17*, 290.
(20) Mulder, T.; Harmandaris, V. A.; Lyulin, A. V.; Van der Vegt, N. F. A.; Michels, M. A. J. *Macromol. Theory Simul.* **2008**, *17*, 393.
(21) Mavrantzas, V. G.; Boone, T. D.; Zervopoulou, E.; Theodorou, D. N. *Macromolecules* **1999**, *32*, 5072.
(22) Robyr, P.; Tomaselli, M.; Grob-Pisano, C.; Meier, B. H.; Ernst, R. R.; Suter, U. W. *Macromolecules* **1995**, *28*, 5320.
(23) Brüning, R.; Samwer, K. *Phys. Rev. B* **1992**, *46*, 11318.
(24) Lyulin, A. V.; Balabaev, N. K.; Michels, M. A. J. *Macromolecules* **2003**, *36*, 8574.
(25) Press, W. H.; Flannery, B. P.; Teukolsky, S. A.; Vetterling, W. T. *Numerical Recipes*; Cambridge University Press: Cambridge, 1985.
(26) Mondello, M.; Yang, H. J.; Furuya, H.; Roe, R. J. *Macromolecules* **1994**, *27*, 3566.
(27) Vorselaars, B.; Lyulin, A. V.; Michels, M. A. J. *Macromolecules* **2007**, *40*, 6001.
(28) Allen, M. P.; Tildesley, D. J. *Computer Simulation of Liquids*; Clarendon Press: Oxford, 1987.
(29) Lemak, A. S.; Balabaev, N. K. *J. Comput. Chem.* **1996**, *17*, 1685.
(30) Mark, J.; Ngai, K.; Graessley, W.; Mandelkern, L.; Samulski, E.; König, J.; Wignall, G. *Physical Properties of Polymers*; Cambridge University Press: Cambridge, UK, 2003.
(31) Flory, P. J. *Statistical Mechanics of Chain Molecules*; Hanser Publishers: New York, 1989.
(32) Dunbar, M. G.; Novak, B. M.; Schmidt-Rohr, K. *Solid State Nucl. Magn. Reson.* **1998**, *12*, 119.
(33) Robyr, P.; Gan, Z.; Suter, U. W. *Macromolecules* **1998**, *31*, 8918.
(34) Robyr, P.; Müller, M.; Suter, U. W. *Macromolecules* **1999**, *32*, 8681.
(35) Gan, Z.; Ernst, R. R. *Chem. Phys. Lett.* **1996**, *13*, 253.
(36) Neuhaus, D.; Williamson, M. P. *The Nuclear Overhauser Effect in Structural and Conformational Analysis*; VCH Publishers: New York, 1989.

MA800873Z